Temporal and Spectral Characteristics of Short Bursts from the Soft Gamma Repeaters 1806-20 and 1900+14

Ersin Göğüş[1,2], Chryssa Kouveliotou[2,3], Peter M. Woods[2,3], Christopher Thompson[4], Robert C. Duncan[5], Michael S. Briggs[1,2]

ABSTRACT

We study the temporal and coarse spectral properties of 268 bursts from SGR 1806−20 and 679 bursts from SGR 1900+14, all observed with the Rossi X-Ray Timing Explorer/Proportional Counter Array. Hardness ratios and temporal parameters, such as T_{90} durations and τ_{90} emission times are determined for these bursts. We find a lognormal distribution of burst durations, ranging over more than two orders of magnitude: $T_{90} \sim 10^{-2}$ to $\gtrsim 1$ s, with a peak at ~ 0.1 s. The burst light curves tend to be asymmetrical, with more than half of all events showing rise times $t_r < 0.3\ T_{90}$. We find that there exists a correlation between the duration and fluence of bursts from both sources. We also find a significant anti-correlation between hardness ratio and fluence for SGR 1806−20 bursts and a marginal anti-correlation for SGR 1900+14 events. Finally, we discuss possible physical implications of these results within the framework of the magnetar model.

Subject headings: X-rays: bursts – gamma rays: bursts – stars: individual (SGR 1806−20) – stars: individual (SGR 1900+14)

1. Introduction

Soft gamma repeaters (SGRs) are a small class of objects that are characterized by brief and very intense bursts of soft gamma-rays and hard X-rays. They are distinguished

[1]Department of Physics, University of Alabama in Huntsville, Huntsville, AL 35899

[2]NASA Marshall Space Flight Center, NSSTC SD-50, 320 Sparkman Dr., Huntsville, AL 35805

[3]Universities Space Research Association

[4]Canadian Institute for Theoretical Astrophysics, 60 St. George St., Toronto, ON, Canada M5S 3H8

[5]Department of Astronomy, University of Texas, RLM 15.308, Austin, TX 78712-1083

from classical gamma-ray bursts (GRBs) by their repeated periods intense activity, during which dozens of bursts with energies approaching 10^{41} ergs are recorded. SGR bursts have significantly softer spectra than classical GRBs; the former are being well fit by an optically-thin thermal bremsstrahlung model with temperatures $kT = 20 - 40$ keV. Two SGRs (0526-66 and 1900+14) have emitted one giant flare each: events that are much more energetic ($E \sim 10^{44-45}$ erg) and contain a very hard spectral component within the first ~ 1 s (Mazets et al. 1979; Cline et al. 1981; Hurley et al. 1999; Mazets et al. 1999; Feroci et al. 1999). For a review of the burst and persistent emission properties of SGRs, see Hurley (2000).

In 1992, it was suggested that SGRs are strongly magnetized ($B \gtrsim 10^{14}$ G) neutron stars, or magnetars (Duncan & Thompson 1992, see also Pacżynski 1992). This model suggests crustquakes as a plausible trigger for the short SGR bursts (as well as the giant flares): a sudden fracture of the rigid neutron star crust, driven by the build-up of crustal stresses as the strong magnetic field gradually diffuses through the dense stellar matter (Thompson & Duncan 1995 [hereafter TD95]; 1996). The motion of the crust shears and twists the external magnetic field, and in the process releases both elastic and magnetic energy.

Cheng et al. (1996) studied a set of 111 SGR 1806−20 bursts (detected with the International Cometary Explorer, ICE) and determined that some of their properties, such as size and cumulative waiting-time distributions are similar to those of earthquakes. Recently, Göğüş et al. (2000) confirmed these similarities for SGR 1806−20 using a larger sample of 401 bursts (111 detected with the Burst and Transient Source Experiment, BATSE, aboard the Compton Gamma Ray Observatory, CGRO; 290 with the the Proportional Counter Array, PCA, on the Rossi X-ray Timing Explorer, RXTE). The same similarities were found for SGR 1900+14 when we analyzed a sample of 1024 bursts (187 observed with CGRO/BATSE; 837 with the RXTE/PCA) (Göğüş et al. 1999). Furthermore, we reported evidence for a correlation between duration and fluence for the SGR 1900+14 bursts, similar to the correlation seen between the duration of strong ground motion at short distances from an earthquake region and the seismic moment ($\propto$ energy) of an earthquake (Lay & Wallace 1995). This similarity strongly suggests that SGR bursts, like earthquakes, may be manifestations of self-organized critical systems (Bak, Tang & Wiesenfeld 1988), lending support to the hypothesis that SGR bursts involve the release of some form of stored potential energy.

Statistical studies such as the above provide important clues not only about the mechanism by which energy is injected during an SGR burst, but also the mechanism by which it is radiated. For example, in the magnetar model the stored potential energy may be predominantly magnetic, and the electrical currents induced by crustal fractures may be strongly localized over small patches of the star's surface, somewhat as they are in solar flares. In such a situation, the energy density in the non-potential magnetic field is high enough that

excitation of high frequency Alfvén motions leads to rapid damping and the creation of a trapped fireball (through a cascade to high wavenumber: Thompson & Blaes 1998). By contrast, if energy is injected more globally, then an approximate balance between injection and radiation will occur in the bursts of luminosity less than $\sim 10^{42}$ erg s^{-1} (Thompson et al. 2000).

Here, we investigate detailed temporal characteristics of a large subset of SGR 1806−20 and SGR 1900+14 bursts observed with the RXTE/PCA during their burst active periods in 1996 and 1998, respectively. We apply to the SGR bursts some temporal analysis methods that were originally developed for the study of GRBs. We also study the spectral variations of the bursts as a function of the burst fluence and duration. In § 2, we briefly review the RXTE/PCA observations. Section 3 describes the data analysis techniques and our results are discussed in § 4.

2. Observations

The PCA instrument (Jahoda et al. 1996) consists of five Xe proportional counter units (PCUs) sensitive to energies between 2−60 keV with 18% energy resolution at 6 keV. The PCA has a total effective area of ~ 6700 cm^2.

SGR 1806−20 : The RXTE/PCA observations of SGR 1806−20 were performed during a burst active period of the source in 1996 (between November 5 and 18) for a total effective exposure time of 136.8 ks. Using the burst search procedure described in Göğüş et al. (2000), we have identified 290 bursts from the source. The number of integrated counts (2−60 keV) for these bursts range between 22 and 34550. Using the count-to-energy conversion factor given in Göğüş et al. (2000) this corresponds to burst fluences between 1.2×10^{-10} and 1.9×10^{-7} ergs cm^{-2} (E > 25 keV). Assuming isotropic burst emission, the corresponding energy range is 3.0×10^{36} – 4.9×10^{39} ergs, for a distance to SGR 1806−20 of 14.5 kpc (Corbel et al. 1997). To facilitate our analysis, we chose events that were clustered together during two very active epochs of the source, resulting in 268 events recorded on 5 (MJD 50392) and 18 (MJD 50405) November 1996.

SGR 1900+14 : RXTE observations of SGR 1900+14 took place between 1998 June 2 and December 21, for a total effective exposure time of 224.1 ks. Using the same burst search algorithm as before, we identified a total of 837 bursts from the source with integrated counts ranging between 22 and 60550. The fluences of these bursts range from 1.2×10^{-10} to 3.3×10^{-7} ergs cm^{-2} (E > 25 keV) corresponding to an energy range of 7×10^{35} – 2×10^{39} ergs (assuming isotropic emission at 7 kpc [Vasisht et al. 1994]). Similarly, we selected 679

events which occurred during a very active period of the source between 1998 August 29 (MJD 51054) and September 2 (MJD 51058).

3. Data Analysis and Results

3.1. Duration (T_{90}) estimates

Originally defined for cosmic GRBs, the T_{90} duration of a burst is the time during which 90% of the total (background-subtracted) burst counts have been accumulated since the burst trigger (Kouveliotou et al. 1993). We calculated the T_{90} duration of SGR bursts using event-mode PCA data (2-60 keV) with 1/1024 s time resolution. For each burst we collected the cumulative counts for an 8 s continuous stretch of data starting 4 s before its peak, t_p. We then fit the cumulative count distribution between two user-selected background intervals [6] with a first order polynomial plus a step function (for the burst) and subtracted the background counts. By using a first order polynomial to fit the cumulative counts, we assume the PCA background remains flat over each 8 s segment. The resulting height of the step function gives the total burst counts. Figure 1 depicts the steps of the T_{90} estimate procedure for one of the SGR 1900+14 bursts.

As the selected bursts occurred during extremely active periods (for both sources), there were quite a number of cases where bursts were clustered very close together. During these active episodes, many crustal sites on the neutron star may be active, releasing stored potential energy in the form of bursts with a large variety of time profiles. Hence, it is important to distinguish single pulse events from events with multiple peaks (which may involve multiple fracture sites). To do this, we applied arbitrary but consistent criteria to our data. We classified an event as *multi-peaked* if the count rate at any local minimum (in 7 ms time bins) is less than half the maximum value attained subsequently in the burst (see Figure 2, middle plots). Otherwise the event was classified as *single-peaked* (Figure 2, top plots). When the count rate dropped to the noise level between peaks, the event was classified as a single, multi-peaked burst if and only if the time between peaks was less than a quarter of the neutron star rotation period (1.3 s for SGR 1900+14, 1.9 s for SGR 1806-20; see Figure 2, bottom plots). We found that 262 of the 679 bursts from SGR 1900+14, and 113 of the 268 SGR 1806-20 bursts were multi-peaked by these criteria. Note that the total counts per burst (or "count fluences") were found to span nearly the same range in the two

[6] Approximately equal background intervals were selected before and after the burst, except in cases where separation between bursts was too small; there we chose smaller, but significant, post/pre burst intervals.

classes of bursts, in both sources. This suggests that the light curve peak structure does not correlate strongly with total energy.

In the context of cosmic GRBs, the value of T_{90} can be systematically underestimated in faint events due to low signal-to-noise (Koshut et al. 1996). We investigated this effect in our SGR analysis using extensive numerical simulations. We created three time profiles based upon the observed time profiles; a single two-sided Gaussian (with right-width twice the left width), two two-sided Gaussians whose peaks are separated by 0.5 s and the peak rate of the second pulse is 0.6 of the first one, and two two-sided Gaussians with peak separation of 1 s. For each profile, we varied the peak rates (eight values between 2600 counts s^{-1} and 55000 counts s^{-1}) and the width of the Gaussians (eight values from 12 ms to 120 ms). We determined the T_{90} duration for each combination before adding noise. Then for each combination, we generated 800 realizations including Poisson noise and determined the respective T_{90} values for these simulations. We found that the fractional difference, FD = 1 − ($T_{90,s}$ / $T_{90,a}$) between the actual value, $T_{90,a}$, (in the absence of noise) and the simulated one, $T_{90,s}$, has a strong dependence on the peak rate (i.e. signal-to-noise ratio), such that FD can be as high as 0.22 at count rates of 2600 counts s^{-1}. It is, however, less than 0.05 for count rates greater than 4800 counts s^{-1}. The variation of FD with respect to the pulse profile is insignificant. Using the results of our simulations we obtained a T_{90} correction as a function of peak rate. We estimated the peak rate of each burst using a box-car averaging technique with a box width of 1/512 s. We then corrected T_{90} values for the S/N effect using our correction function and these peak rates.

Our final data set thus comprises 455 SGR 1900+14 bursts with corrected T_{90} durations between 9 ms and 2.36 ms (Figure 3, solid histogram). We were unable to determine statistically significant T_{90} durations for 187 SGR 1900+14 bursts because there were less than ~ 40 counts per event. The solid curve in Figure 3 is a best fit log-Gaussian function to all T_{90} values which peaks at 93.9 ± 0.2 ms ($\sigma = 0.35 \pm 0.01$; where σ is the width of the distribution in decades). The dashed histogram in Figure 3 is the distribution of T_{90} values of single pulse bursts whose log-Gaussian mean is 46.7 ± 0.1 ms ($\sigma = 0.21 \pm 0.01$). Also in Figure 3, the dash-dot histogram displays the T_{90} distribution of multi-peaked bursts and it peaks at 148.9 ± 0.2 ms ($\sigma = 0.26 \pm 0.02$). For SGR 1806−20 bursts, we determined corrected T_{90} values of 190 bursts which range between 16 ms and 1.82 s (49 bursts were too weak to determine their T_{90} values). The distribution of all T_{90} values is shown in Figure 4 (solid histogram). A log-Gaussian fit to this distribution yields a peak at 161.8 ± 0.2 ms ($\sigma = 0.34 \pm 0.02$). Similarly, a log-Gaussian fit to the T_{90} distribution of the single pulse bursts (dashed lines in Figure 4) peaks at 88.1 ± 0.1 ms ($\sigma = 0.19 \pm 0.03$) and a fit to the multi-peaked bursts (dash-dot lines in Figure 4) yields a peak at 229.9 ± 0.3 ms ($\sigma = 0.32 \pm 0.03$).

In order to quantify the time profile symmetry of SGR bursts we determined the ratio of their rise times (t_r, i.e. the interval between T_{90} start time and peak time t_p) to T_{90} durations of the single pulse events. In Figure 5, we plot the distributions of these ratios for bursts with single pulse (solid histogram) and milti-peaks (dashed histogram) from SGR 1900+14 (left) and those from SGR 1806−20 (right). The majority of single pulse events from both sources have t_r / T_{90} values less than 0.3, showing that SGR bursts decay slower than they rise, or in other words that SGR pulse profiles are asymmetric. We find that the average values os the t_r / T_{90} ratios are 0.29 and 0.27 for SGR 1900+14 and SGR 1806−20, respectively. Remarkably coincident average values, along with very similar distributions of t_r / T_{90} ratios of both sources suggest a similarity of the asymmetry in the temporal profiles of SGR bursts.

3.2. Emission time (τ_{90}) estimates

Emission time, τ_N, was introduced for cosmic GRBs as a complimentary temporal parameter to T_{90} (Mitrofanov et al. 1999). Emission time is the time over which a fixed percentage, N%, of the total burst emission was recorded, starting from the peak of the event and moving downward in flux. For each burst, we determined the average background level from the background intervals used in the T_{90} estimating procedure. The background-subtracted count bins within the burst interval (i.e. from the end of pre-burst background range to the beginning of post-burst background range) were then ordered by decreasing count rate. Starting with the highest count rate bin (i.e. the peak), we added the counts of each successively weaker bin until 90% of the total burst counts were accumulated. The τ_{90} emission time of the burst is then the total time spanned by the accumulated bins.

As with the T_{90} parameter, when the S/N ratio of the burst is low, the measured emission time can be systematically smaller than the actual value (Mitrofanov et al. 1999). In order to correct for this systematic error, we constructed numerous simulated profiles identical to those described in the previous section. We found that, similar to T_{90} estimates, the FD between the actual and simulated τ_{90} emission times is strongly dependent on the peak rate. FD is ~ 0.26 at count rates of 2600 counts s^{-1} and less than 0.06 for count rates greater than 4800 counts s^{-1}. Similar to the T_{90} measurement, this effect is only weakly dependent on the temporal profile of the burst. Using our τ_{90} correction function and the peak rates, we obtained the corrected τ_{90} emission times. The corrected values range between 4.6 and 412.8 ms for SGR 1900+14 bursts, and between 4.8 and 559.2 ms for SGR 1806−20 bursts. In Figure 6, we show the distributions of τ_{90} emission times for SGR 1900+14 (*left*) and SGR 1806−20 (*right*). The dashed lines in both plots are the best fit log-Gaussian curves

which peak at 49.6 ± 0.1 ms ($\sigma = 0.28 \pm 0.01$) for SGR 1900+14 events, and at 82.3 ± 0.1 ms ($\sigma = 0.32 \pm 0.02$) for SGR 1806−20 events. The τ_{90} emission times of bursts from both sources are on average shorter than T_{90} durations. Note that the log-Gaussian mean values of T_{90} distributions of *single* pulse bursts from both SGRs are quite similar to those of the τ_{90} distributions.

3.3. Duty cycles (δ_{90})

As shown in the previous section, the τ_{90} values of bursts are in general smaller than their T_{90} values. The reason is that τ_{90} is not a measure of the actual duration of the burst when the morphology of the burst is complex (e.g. multiple peaks). Mitrofanov et al. (1999) suggested that the ratio τ_{90}/T_{90} can then be used to describe a duty cycle, δ_{90}. We, therefore, determined the δ_{90} parameters for all bursts of both sources (Figure 7, *left* for SGR 1900+14 bursts, *right* for SGR 1806−20 bursts). Both distributions peak at about $\delta_{90} \sim 0.45$ and their overall shapes are very similar, indicating a strong similarity of the *type* of burst emission in the two sources, although their overall duration distribution differ.

3.4. Duration – Fluence – Hardness correlations

Gutenberg and Richter (1956) showed that there exists a power law relation between the magnitude (which is related to the total energy involved) of earthquakes and the durations of strong ground-shaking at short distances from an earthquake epicenter. We investigated whether a similar correlation exists in SGR events using their total burst counts and their T_{90} durations (as estimated in §3.1), for both SGR 1806−20 and SGR 1900+14. For each set of bursts, we grouped the T_{90} values into logarithmically spaced bins and determined the weighted mean value of total burst counts and T_{90} durations for each bin. In Figure 8, we show the plot of integral counts vs T_{90} durations of SGR 1806−20 bursts. The crosses in this figure are the weighted means of each parameter; the errors on the mean-T_{90} values denote the range of each bin while the errors on the mean counts are due to sample variance. The dark points are the individual measurements of the burst counts and T_{90} values of single pulse events and the gray circles are those of multi-peaked bursts. Figure 8 shows that the integral counts and durations of SGR 1806−20 bursts are well correlated. To quantify this correlation, we determined the Spearman's rank order correlation coefficient, $\rho = 0.91$, and the probability of getting this value from a random data set, P=3.4×10^{-4}. We further fit a power law model to the mean values (crosses) of the data using the least squares technique, which yields a power law index of 1.05 ± 0.16.

Similarly, Figure 9 shows that the integral counts and T_{90} durations of SGR 1900+14 bursts are also correlated, having $\rho = 0.89$ and P $= 8.6 \times 10^{-4}$. A power law fit to the mean values of the data yields an index of 0.91 ± 0.07. The asterisk shown in the upper right portion of Figure 9 indicates where the precursor of the August 29 burst falls. This event was exceptionally long, bright and resembled the August 27 giant flare in various ways (Ibrahim et al. 2000). A spectral line at 6.4 keV was reported during the precursor of event of August 29 burst with $\sim 4\ \sigma$ significance (Strohmayer & Ibrahim 2000). If spectral lines are event intensity dependent, there are very few events in Figure 9 during which we would expect to see any lines. The detailed spectral analysis of all SGR bursts is underway.

In conclusion we find a good correlation between the duration and total counts (energy) of SGR bursts, quite similar to the one established for earthquakes. It is noteworthy that the burst count fluences of single pulse events (from both systems) span a range almost as wide as that of fluences of multi-peaked bursts.

In order to investigate burst spectral variations versus fluence, we calculated an event hardness ratio defined as the ratio of the total burst counts observed between 10−60 keV to those between $2 - 10$ keV. Bursts with total counts less than ~ 50 yielded statistically insignificant hardness ratios ($< 3\ \sigma$), and therefore, were excluded from our analysis. For SGR 1806−20 bursts, we have 159 events with hardness ratios measured to $> 3\ \sigma$ accuracy. We divided the total counts of these events into logarithmically spaced bins and determined the weighted mean hardness ratio for each group. Figure 10a shows that the SGR 1806−20 burst hardness ratios are anti-correlated with fluence (ρ=−0.96, P=2.6×10^{-4}). For 385 SGR 1900+14 bursts, Figure 10d shows a marginal anti-correlation between hardness and fluence ($\rho = -0.89$, P=4.6×10^{-3}). Interestingly, we find that although the hardness − fluence anti-correlation is evident in both sources, the SGR 1806−20 events are *overall* harder than the SGR 1900+14 ones. Our energy selection optimizes the PCA energy response, so that we are not affected by instrumental biases.

Fenimore, Laros & Ulmer (1994) have performed a similar study of hardness ratio vs fluence for 95 SGR 1806-20 events detected with ICE. We cannot directly compare our results with this study for two reasons. The energy ranges over which hardness ratios are computed differ significantly; while we use $(10 - 60$ keV$)/(2 - 10$ keV), Fenimore et al. (1994) use $(43.2 - 77.5$ keV$)/(25.9 - 43.2$ keV). The PCA sensitivity drops significantly beyond 25 keV, limiting the possibility of comparison. Furthermore, our fluence range ends at 2×10^{-7} ergs cm^{-2}, just below the range described in Figure 1 of Fenimore et al. (1994). However, since Fenimore et al. report a constant trend above 10^{-7} ergs cm^{-2}, one could postulate that the hardness ratio vs fluence trend we report, levels off at higher fluences (energies).

We further investigated the hardness − fluence trend for burst morphology sub-sets,

namely for single pulse and multi-peaked burst groups for each source. Figure 10b exhibits hardness − fluence plot of single pulse SGR 1806−20 events and Figure 10c shows that of multi-peaked bursts. We see that both sets display spectral softening as the burst count fluence increases. Similarly SGR 1900+14 events are shown in Figure 10e and f. For this source, the hardness − fluence anti-correlation is significant only for single pulse bursts. It is important to note that the peak rates of most of the highest fluence bursts reach $\gtrsim 10^5$ counts s^{-1} (on 1/1024 s time scale) around which the PCA pulse pileup may become important. This effect can artificially harden the observed count spectrum at these rates. The spectral hardening or leveling off seen in the last bins of the plots of Figure 10 may well be due to the pulse pileup effect and should not be considered as intrinsic source property.

We next investigated the relationship between the hardness and duration of SGR bursts. Although we find hardness − fluence anti-correlations and fluence − duration correlations, both SGR 1806−20 (Figure 11, squares) and SGR 1900+14 (Figure 11, diamonds) burst hardness ratios are independent of the event durations.

4. Discussion

Our study demonstrates that unlike the T_{90} duration distribution of cosmic GRBs which shows a bi-modal trend with peaks at ~ 0.31 s and ~ 37 s (Kouveliotou et al. 1993; Paciesas et al. 1999), the T_{90} distribution of SGR bursts displays a single peak which varies for each source: ~ 93 ms and ~ 162 ms for SGR 1900+14 and SGR 1806−20, respectively.

We find that the T_{90} durations of single-pulse bursts from both SGRs form narrow distributions (compared to those of multi-peaked events) which peak at ~ 47 ms and ~ 88 ms for SGR 1900+14 and SGR 1806-20, respectively. These bright, hard, and short bursts are almost certainly powered by a sudden disturbance of the rigid neutron star crust, which transmits energy to the magnetosphere. Magnetic stresses, which force the star between distinct metastable equilibria, provide the most plausible source of energy for the giant flares, and by inference for the short bursts (TD95; Thompson & Duncan 2001).

The duration of the multi-peaked bursts is clearly fixed by the time between successive releases of energy. The widths of the single pulse bursts could, in principle, be limited either by the rate of release of energy from the initial reservoir or, alternatively, by the time for the released energy to be converted to radiation through some intermediate reservoir. There have been various suggestions for such an intermediate storage mechanism: a hot fireball that is confined on closed magnetic field lines (TD95); a region of strong magnetic shear and high current density (Thompson et al. 2000); or a persistent vibration of the star (Fatuzzo

& Melia 1994).

Measurement of the burst rise time t_r provides a discriminant between these possibilities. We find that t_r is characteristically much shorter than the total duration, as defined by either T_{90} or τ_{90}. Moreover, the distribution of t_r/T_{90} is broad (both for single-pulsed bursts and multi-peaked events), which suggests that t_r is not directly connected to cooling. For example, the X-ray luminosity of a trapped fireball in local thermodynamic equilibrium is proportional to its surface area, and is a weak function of its internal temperature (Thompson & Duncan 1995). The characteristic radiative timescales are, in general, very short at the high spectral intensity of an SGR burst. Thus, the rise of the X-ray flux plausibly represents the initial injection of energy, although strictly t_r only sets an upper bound to the injection timescale.

While the overall shape of T_{90} (both single and multi-peaked) and the τ_{90} distributions of both sources are quite similar (relatively consistent Gaussian widths), the peaks of both distributions for SGR 1900+14 occur at shorter durations compared to those for SGR 1806−20. This systematic difference in the burst durations probably results from some differing intrinsic property of the sources, such as the strength of the magnetic field, or the size of the active region.

We find a power law correlation between the total burst counts (fluence) and the duration of SGR bursts with a power law index around 1. Similar behavior was noted for earthquakes by Gutenberg & Richter (1956). Within the context of earthquake mechanics, one way of defining duration (also known as "bracketed duration" [Bolt 1973]) is the time between the first and last 5% excesses of g (gravitational acceleration on Earth) by the threshold acceleration of strong ground shaking. Recently, Lay & Wallace (1995) presented the power law correlation between the seismic moment ($\propto$ energy) and duration of 122 earthquakes with energies between 3.5×10^{23} erg and 2.8×10^{26} erg. The power law fit to these events yields an index of 3.03.

An equally important constraint on the injection and cooling mechanisms comes from the anti-correlation between the hardness and fluence of the SGR bursts. Although very significant for SGR 1806-20, this anti-correlation is much milder than that expected for black-body emission from a region of constant area; indeed, the trend of increasing hardness with lower fluence is opposite to that expected for constant area emission. Two basic types of radiative mechanism could reproduce this trend. First, the emitting plasma could be in local thermodynamic equilibrium, which requires that its size (radiative area) should decrease at lower fluences. An alternative possibility is that the spectral intensity of the radiation field sits below that of a black body, and that the temperature of the emitting plasma is buffered within a narrow range. We consider each of these possibilities in turn.

An SGR burst can be parameterized by the rate of injection of energy into the magnetosphere, $L_{\rm inj}$, and the volume V of the injection region. When $L_{\rm inj}$ is large and V is small enough, it is not possible to maintain a steady balance between heating and radiative cooling. The deposited energy is locked onto closed magnetic field lines of the neutron star, in a "trapped fireball" composed of photons and electron-positron pairs (TD95). This kind of event will tend to have a soft spectrum, because the injected energy has thermalized, and the plasma remains in LTE very close to its photosphere. The rise time is comparable to the time over which energy is initially injected, but the decay is limited by the rate of cooling through a thin radiative surface layer, which contracts toward the center of the fireball. The declining light curve of the 27 August 1998 giant flare can be accurately fit by such a model (Feroci et al. 2001; Thompson & Duncan 2001).

A second burst from SGR 1900+14 on 29 August 1998 has been interpreted in this trapped fireball model (Ibrahim et al. 2000). The main 29 August burst had a much shorter duration than the giant flare (~ 3.5 s versus ~ 400 s). This bright component was followed by a much fainter pulsating tail (extending out to ~ 1000 s) which provides direct evidence for heating and compression of the neutron star surface by the fireball. In this model, the short duration and high luminosity of the bright component require that the trapped fireball had an approximately planar geometry, as would be expected if the energy were released along an extended fault (Ibrahim et al. 2000).

As our results show, most single-pulsed bursts from SGR 1900+14 have a much shorter duration (40 times smaller) than the bright component of the August 29 burst. It remains unclear, therefore, whether the trapped fireball model also applies to these much more frequent events. If it does apply, then the narrowness of the T_{90} distribution (compared with the wide range of measured fluences) also requires a planar geometry, because the cooling time is determined by the smallest dimension of the fireball.

The radiative mechanism is somewhat different if the injection luminosity $L_{\rm inj}$ lies below a critical value of $\sim 10^{42}\,(V^{1/3}/10\ {\rm km})$ ergs s^{-1} (assuming a spherical geometry; Thompson & Duncan 2001). When the compactness is that low, it is possible to maintain a steady balance between the heating of a corona of electron-positron pairs, and radiative diffusion out of the corona (which one deduces must be optically thick to scattering). The central temperature of the corona is buffered in the range $\sim 20 - 40$ keV, and remains higher at *lower* luminosities – just the trend observed for SGR 1806-20 (Fig. 10). If this radiative model applies to the majority of single-pulsed events, then the constraints on the geometry of the active region are weaker, and one must consider alternative mechanisms for storing the injected energy, such as a persistent current driven by shearing motions in the neutron star crust (Thompson et al. 2000).

E.G. is grateful to James C. Pechmann for useful discussions on earthquakes. We acknowledge support from NASA grants NAG5-6021, NAG5-7785(E.G); the LTSA grant NAG 5-9350 (P.M.W. & C.K.); NASA grant NAG5-3100 and Alfred P. Sloan foundation (C.T.); the Texas Advanced Research Project grant ARP-028 and NASA grant NAG5-8381 (R.C.D.). Several of the ideas presented in this work originated at the ITP funded by NSF grant PHY99-07949.

REFERENCES

Bak, P., Tang, C. & Wiesenfeld, K. 1988, Phys. Rev. A, 38, 364

Bolt, B.A. 1973, in 5th World Conf. Earthquake Eng., Inter. Assoc. for Earthquake Eng., Rome, paper no. 292

Cheng, B., et al. 1996, Nature, 382, 518

Cline, T.L., et al. 1981, ApJ, 255, L45

Corbel, S., et al. 1997, ApJ, 478, 624

Duncan, R.C. & Thompson C. 1992 ApJ, 392, L9

Fatuzzo, F, & Melia, F. 1994, in AIP Proc., 2th Huntsville Symp. on Gamma-Ray Bursts, eds. G.J. Fishman, J.J. Breinerd & K. Hurley (New York: AIP), p.515

Fenimore, E.E., Laros, J.G. & Ulmer, A. 1994, ApJ, 432, 742

Feroci, M., et al. 1999, ApJ, 515, L9

Feroci, M., Hurley, K., Duncan, R.C., & Thompson C. 2001, ApJ, in press, astro-ph/0010494

Göğüş, E., et al. 1999, ApJ, 526, L93

Göğüş, E., et al. 2000, ApJ, 532, L121

Gutenberg, B. & Richter, C.F. 1956, Bull. Seis. Soc. Am., 46, 105

Hurley, K., et al. 1999, Nature, 397, 41

Hurley, K., et al. 2000, in AIP Proc., 5th Huntsville Symp. on Gamma-Ray Bursts, eds. R.M. Kippen, R.S. Mallozzi & G.J. Fishman (New York: AIP), p.763

Jahoda, K. et al. 1996, Proc. SPIE, 2808, 59

Ibrahim, A., et al. 2001, ApJ, submitted, astro-ph/0007043

Kouveliotou, C., et al. 1993, ApJ, 413, L101

Koshut, T.M., et al. 1996, ApJ, 463, 570

Lay, T. & Wallace, T., eds. 1995, Modern Global Seismology, (San Diego: Academic), p.378

Mazetz, E.P., et al. 1979, Nature, 282, 587

Mazetz, E.P., et al. 1999, Astronomy Letters, 25, 635

Mitrofanov, I.G., et al. 1999, ApJ, 504, 925

Paciesas, W.S., et al. 1999, ApJS, 122, 465

Pacżynski, B. 1992, Acta Astron., 42, 145

Strohmayer, T & Ibrahim, A. 2000, ApJ, 537, 111

Thompson, C. & Duncan, R.C. 1995, MNRAS, 275, 255

Thompson, C. & Duncan, R.C. 1996, ApJ, 473, 322

Thompson, C. & Blaes, O. 1998, Phys. Rev. D, 57, 3219

Thompson, C., et al. 2000, ApJ, 543, 340

Thompson, C. & Duncan, R.C. 2001, ApJ, submitted

Vasisht, G., et al. 1994, ApJ, 431, L35

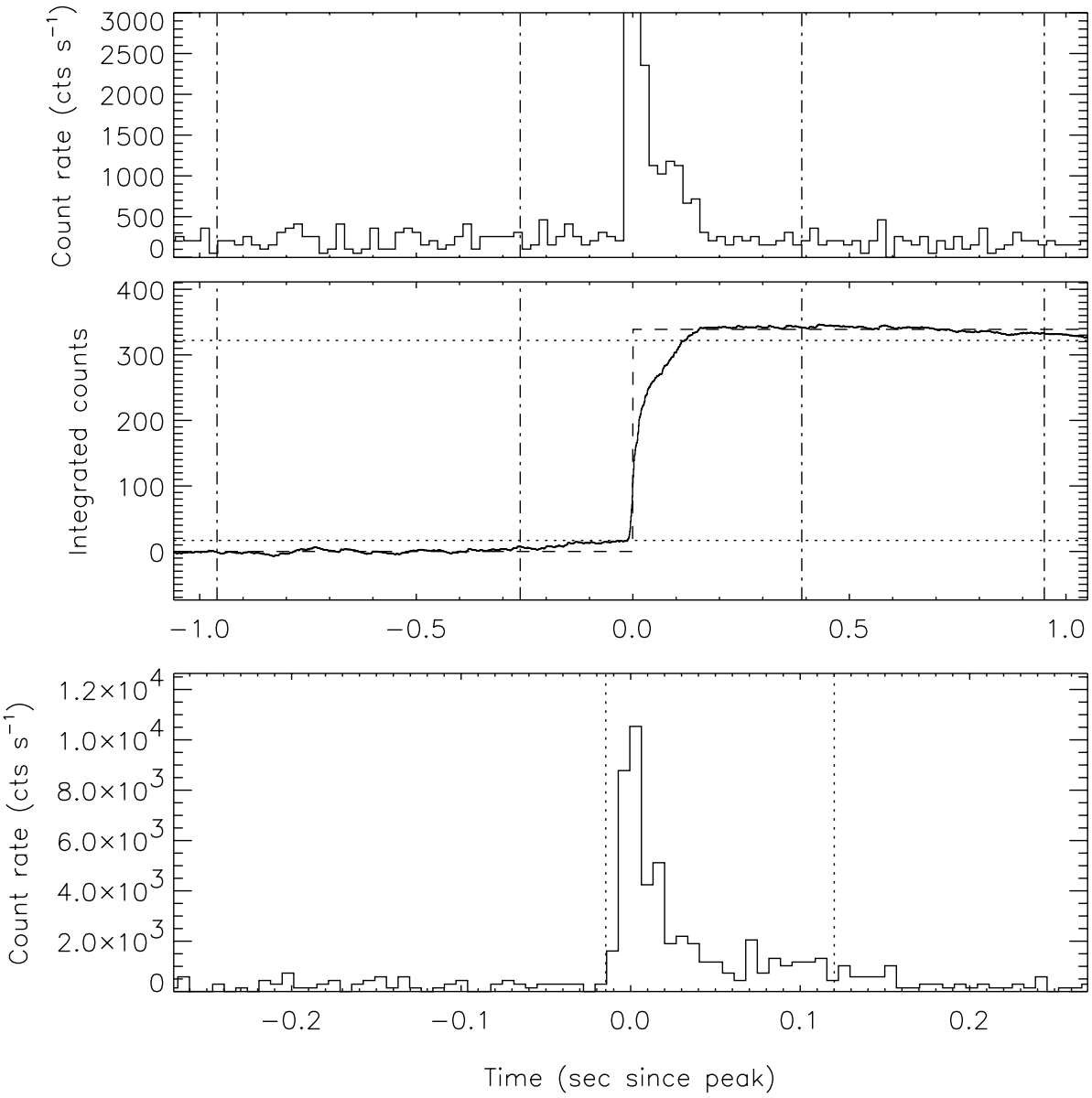

Fig. 1.— (*top panel*) Light curve of a SGR 1900+14 burst (2−60 keV) accumulated with 20 ms time resolution. The vertical dot-dash lines before and after the burst are the boundaries of the selected pre- and post-background intervals. (*middle panel*) The solid line shows the cumulative counts, with the background contribution (as fit by a first-order polynomial) subtracted off. The dashed line shows a step-function fit to the burst counts. The lower horizontal dotted line represents the 5% and upper horizontal dotted shows the 95% count fluence level. Note that the top and the middle panels are in the same time scale. (*bottom panel*) Time profile of the same burst with 7 ms time resolution and zoomed in near the time of the burst. The vertical dotted lines are the start and the end times of its T_{90} duration.

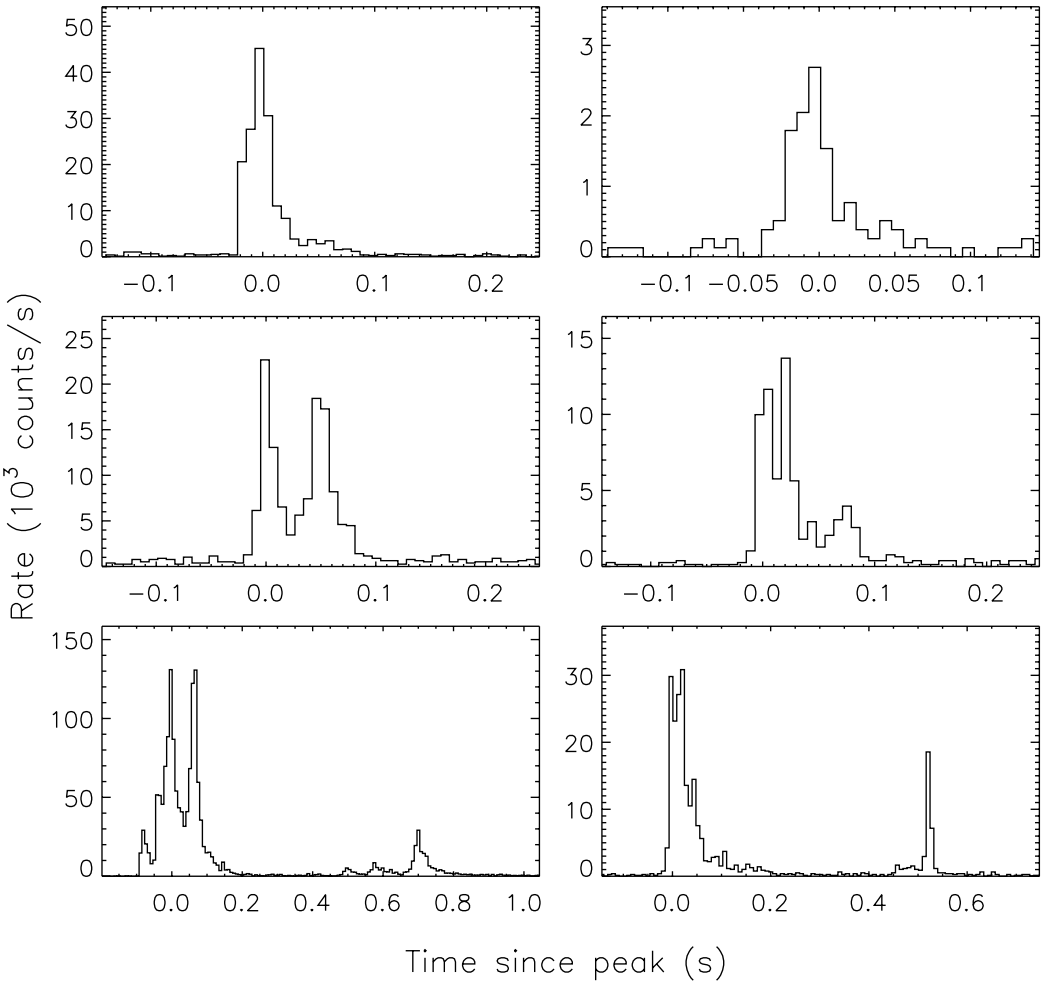

Fig. 2.— Time profiles of some SGR 1900+14 and SGR 1806−20 bursts (on 7 ms time scale) to illustrate single pulse bursts (top plots) and multi-peaked bursts (middle and bottom plots).

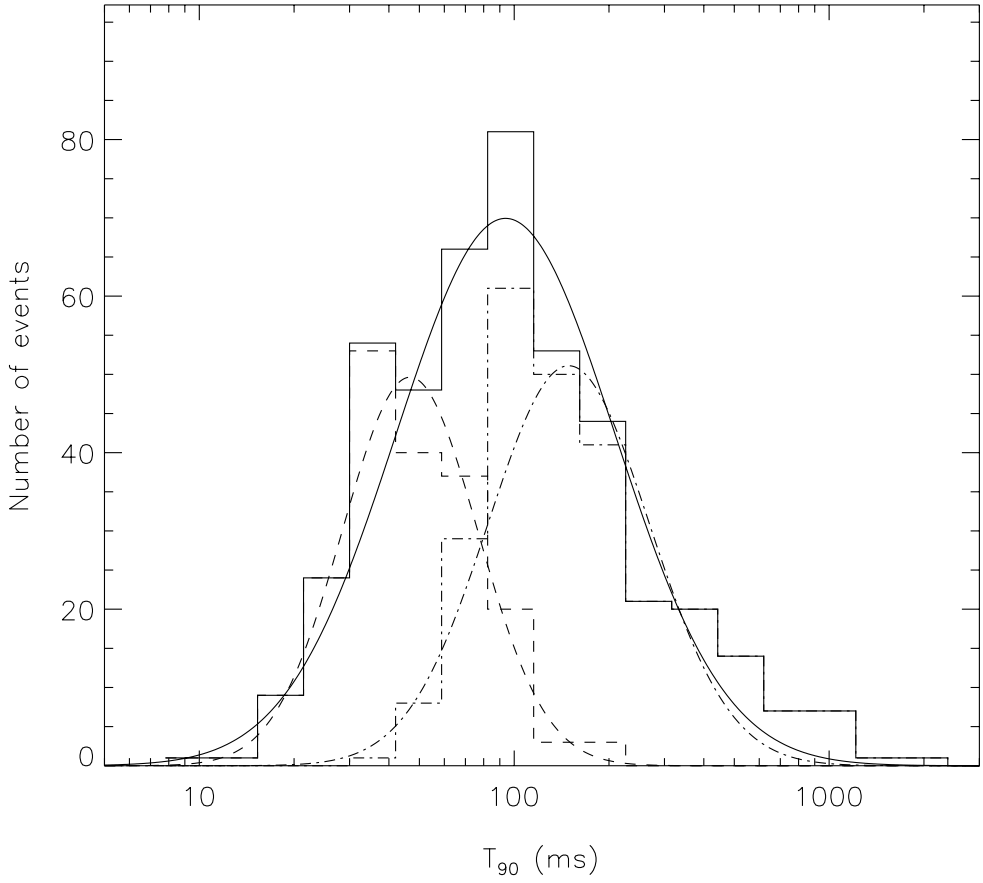

Fig. 3.— Distributions of the T_{90}-durations for all (solid), single pulse (dashed) and multi-peaked (dash-dot) SGR 1900+14 bursts. The solid, dashed and dash-dot curves are obtained by fitting a log-Gaussian model to each set. Sets peak at 93.4 ms, 46.7 ms and 148.9 ms, respectively.

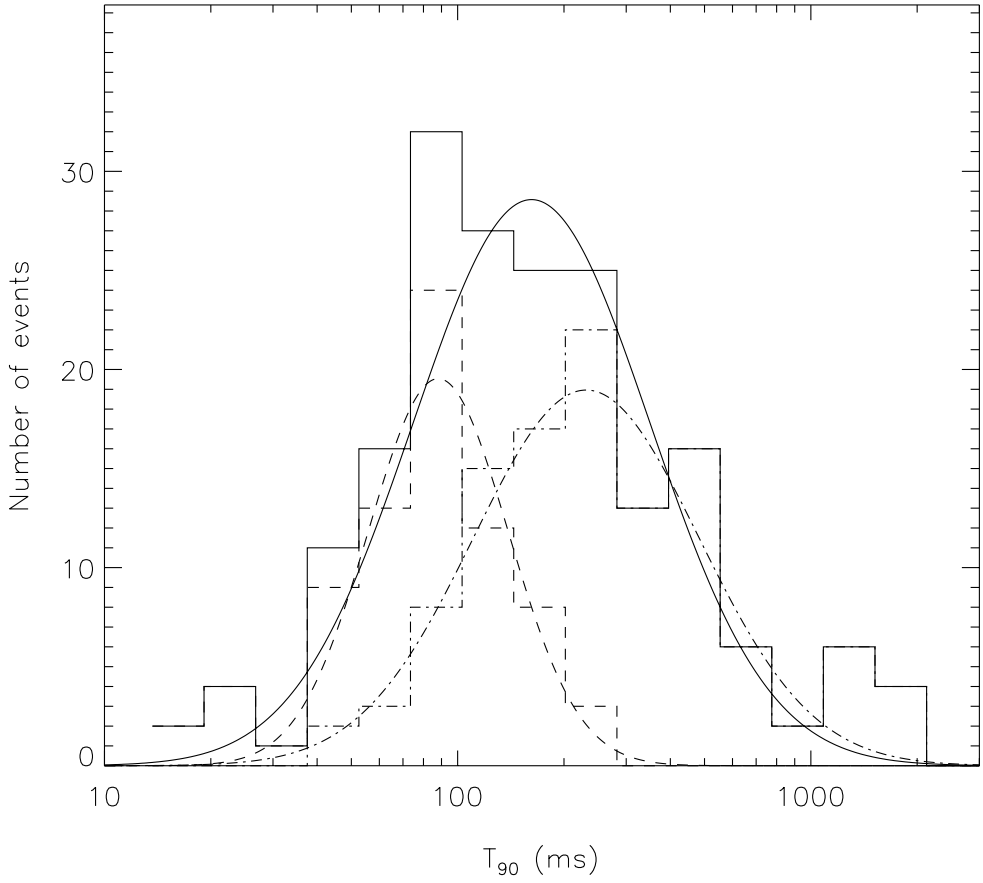

Fig. 4.— Distributions of the T_{90}-durations for all (solid), single pulse (dashed) and multi-peaked (dash-dot) SGR 1806−20 bursts. The solid, dashed and dash-dot curves are obtained by fitting a log-Gaussian model to each set. Sets peak at 161.8 ms, 88.1 ms and 229.9 ms, respectively.

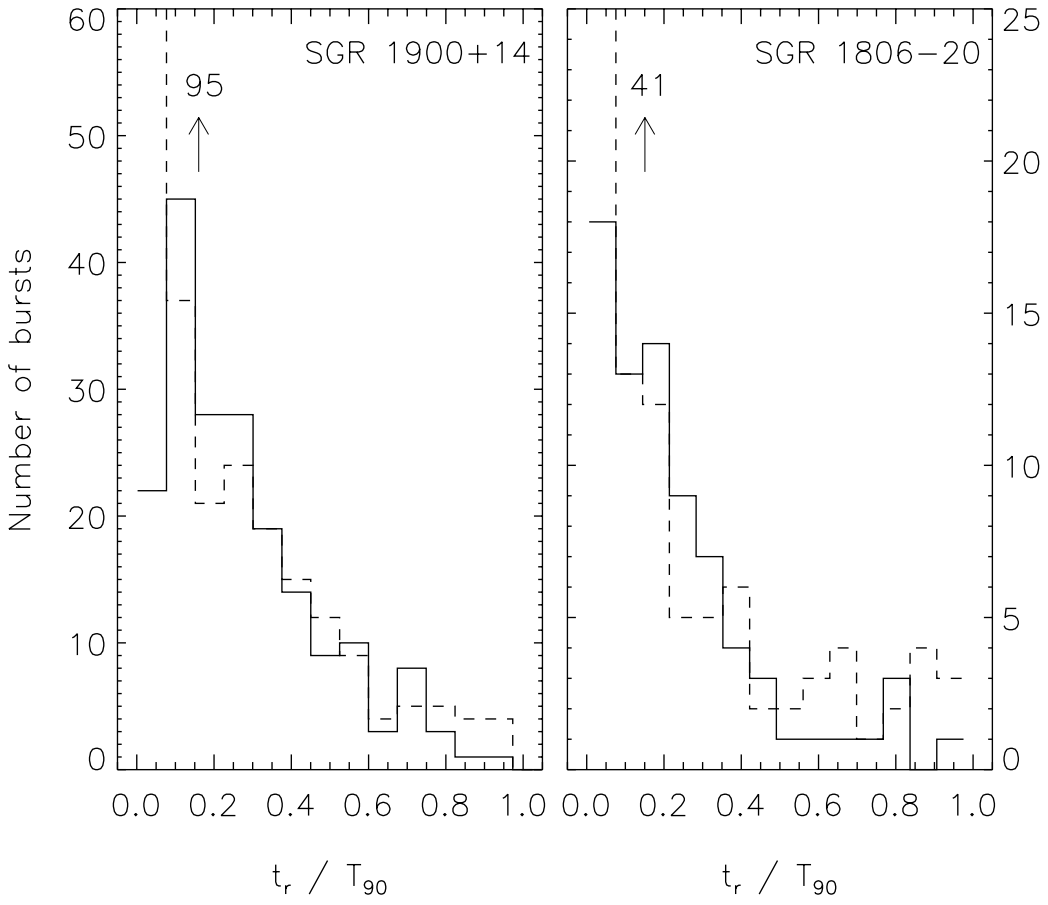

Fig. 5.— Distributions of the ratios of rise times, t_r to T_{90} durations for single pulse bursts (solid) and multi-peaked bursts (dashed) from SGR 1900+14 (left) and SGR 1806−20 (right). Note that the number of multi-peaked events with the lowest t_r/T_{90} ratios is artificially large due to the longer (compared to t_r) durations of these bursts (see Figure 2, middle and bottom plots).

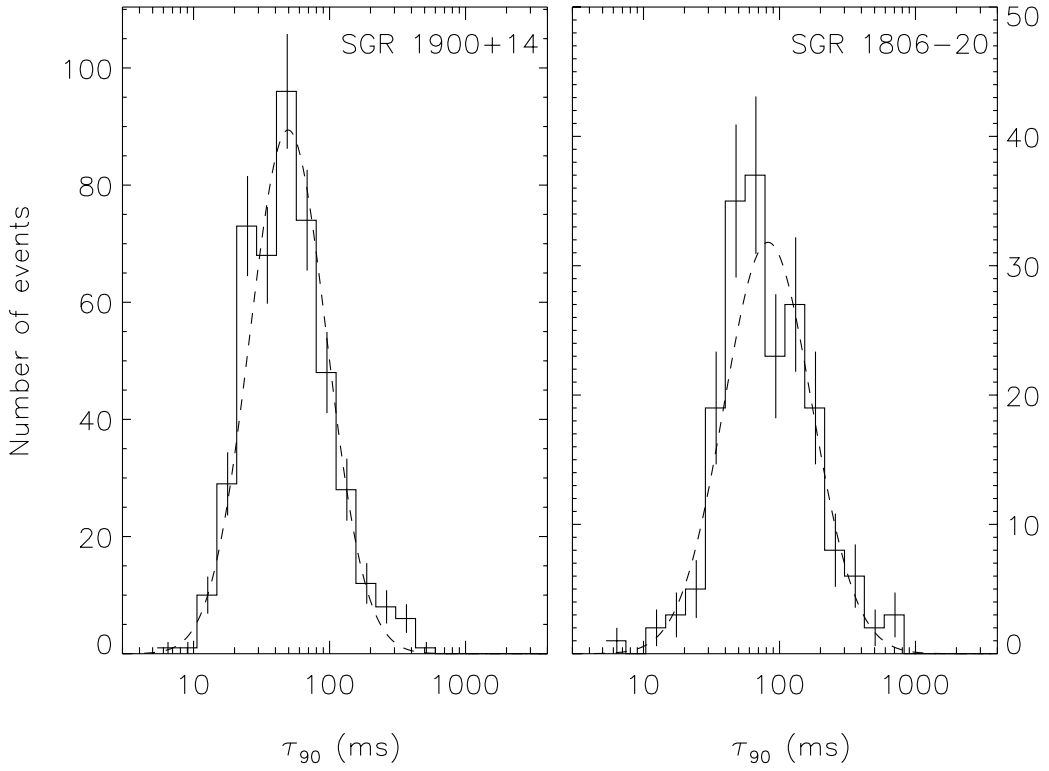

Fig. 6.— Distributions of the τ_{90} emission times for SGR 1900+14 (left) and SGR 1806−20 (right) bursts. The dashed curves are obtained by fitting a log-Gaussian model to each set, with peaks at 49.6 ms and 82.3 ms, respectively.

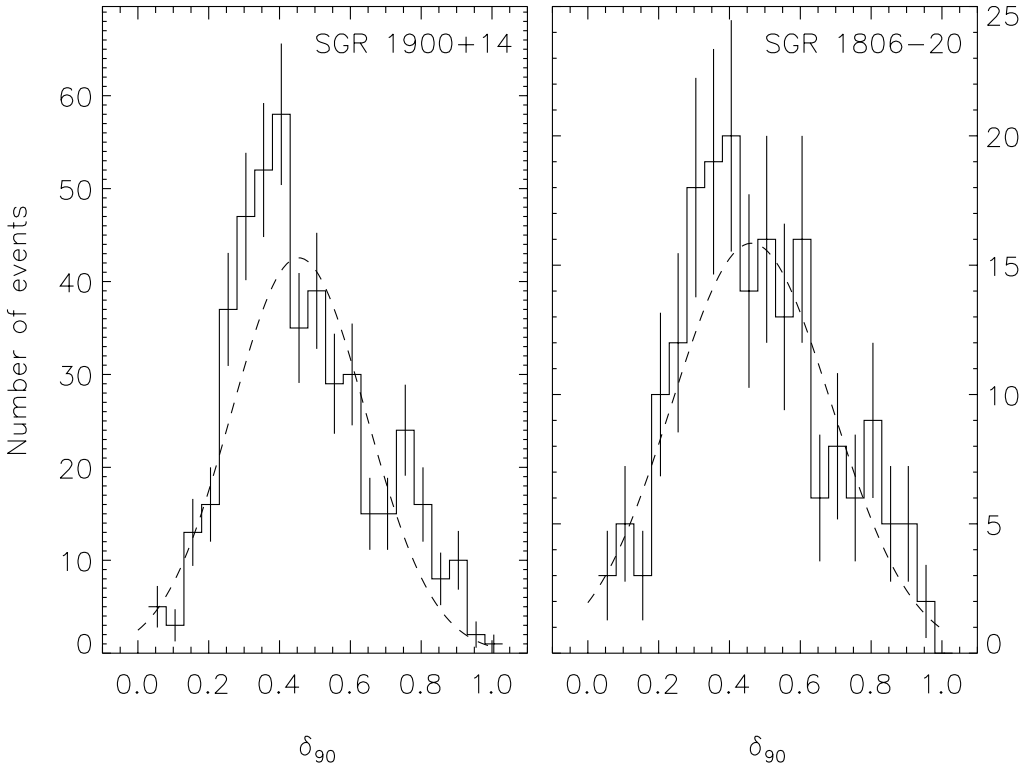

Fig. 7.— Distributions of the duty cycles, δ_{90}, for SGR 1900+14 (left) and SGR 1806−20 (right) bursts. The Gaussian fits peak at 0.45 and 0.46, respectively.

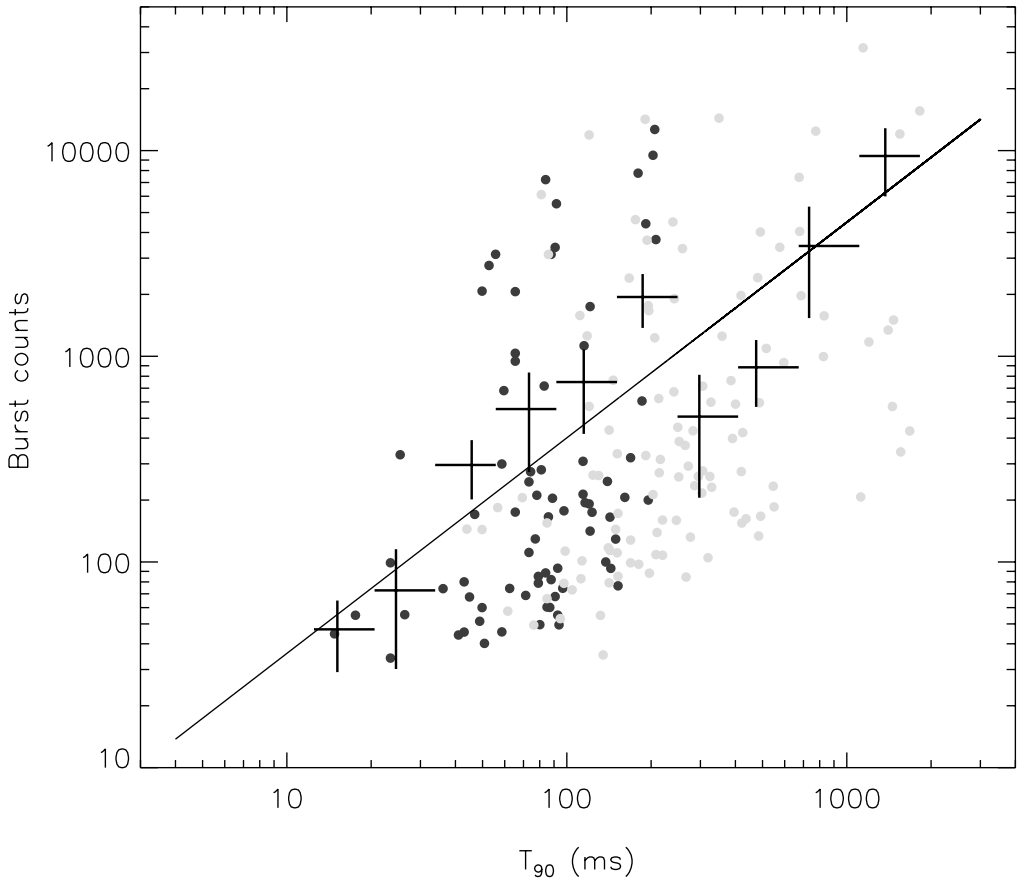

Fig. 8.— Plot of the total counts vs T_{90}-durations for 190 SGR 1806− 20 bursts which shows a correlation (ρ = 0.91, P=3.4 × 10^{-4}). The solid line is obtained by fitting a power law model to the crosses (which are explained in the text). The best fit power law index is 1.05 ± 0.16. The circles are the individual measurements for single pulse (dark) and multi-peaked (gray) bursts.

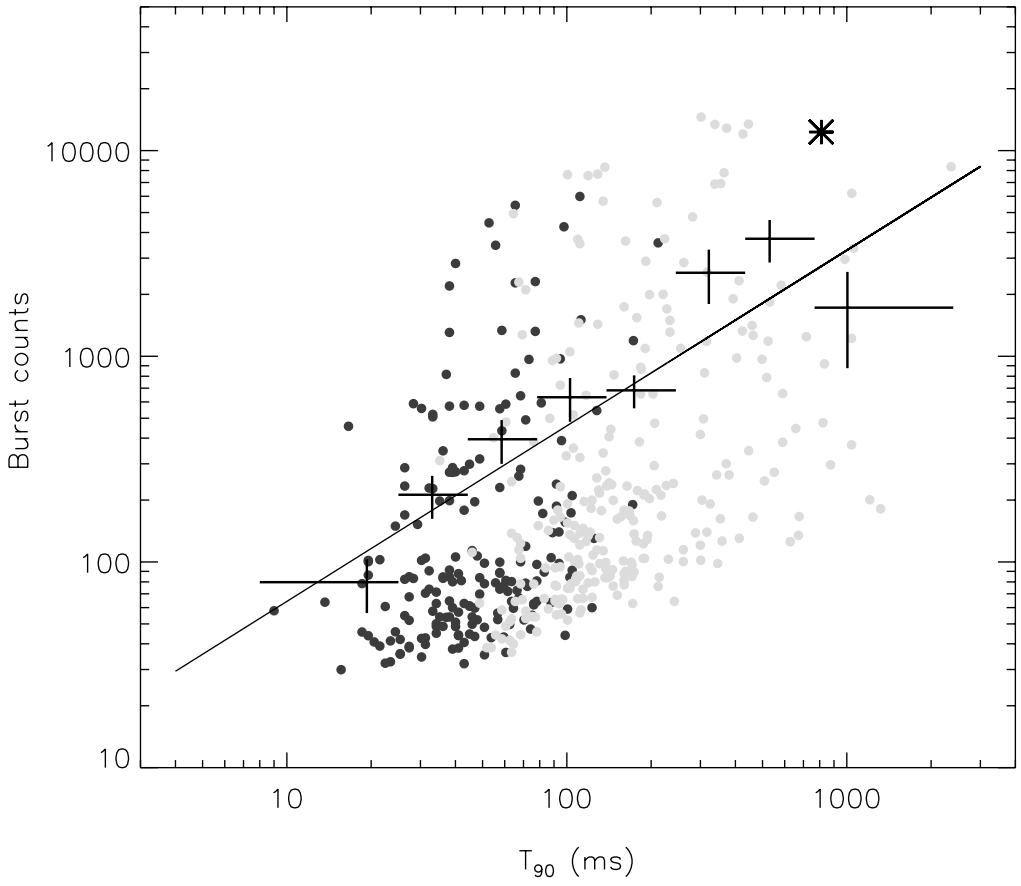

Fig. 9.— Plot of the total counts vs the T_{90}-durations for 455 SGR 1900+14 bursts which shows a correlation ($\rho = 0.89$ and $P = 8.6 \times 10^{-4}$). A power law fit to the crosses (solid line) yields an index of 0.91 ± 0.07. The asterisk indicates where August 29 precursor would be seen. The circles represent the measured values for single pulse (dark) and multi-peaked (gray) bursts.

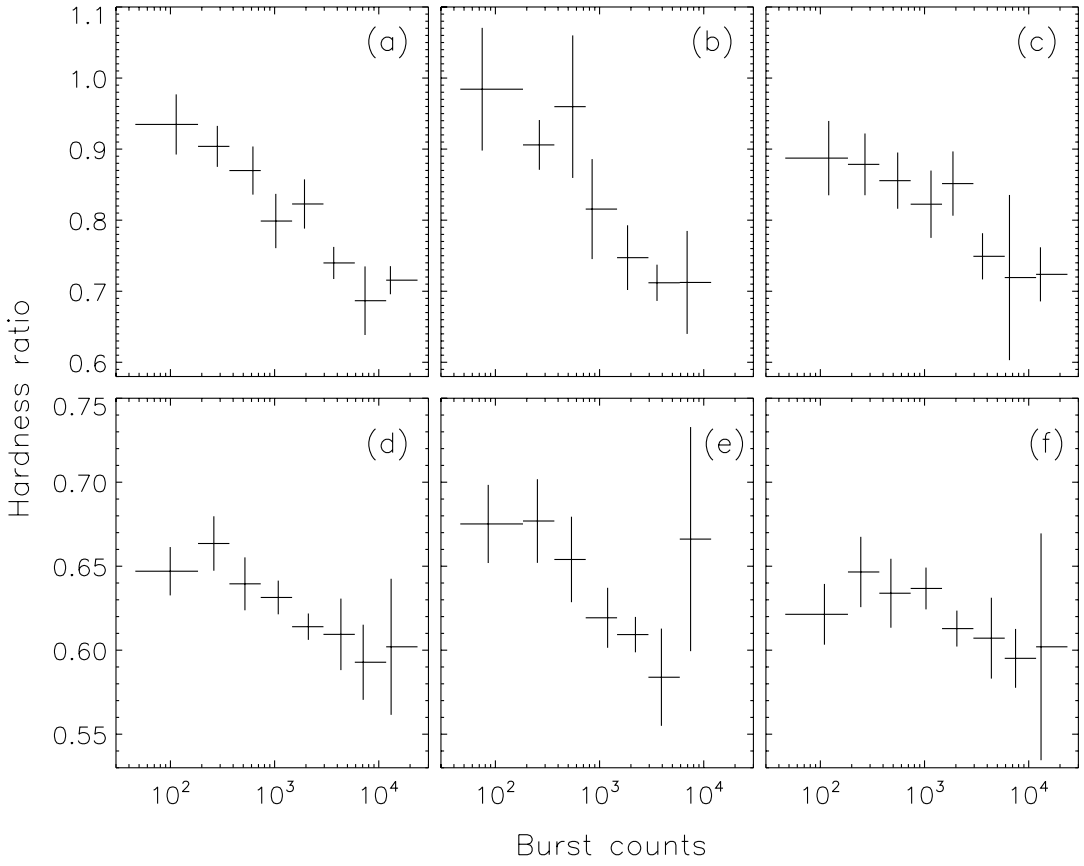

Fig. 10.— Plot of hardness ratios vs total counts for (a) all, (b) single pulse, (c) multi-peaked SGR 1806−20 bursts. Similarly, those for (d) all, (e) single pulse, (f) multi-peaked SGR 1900+14 events.

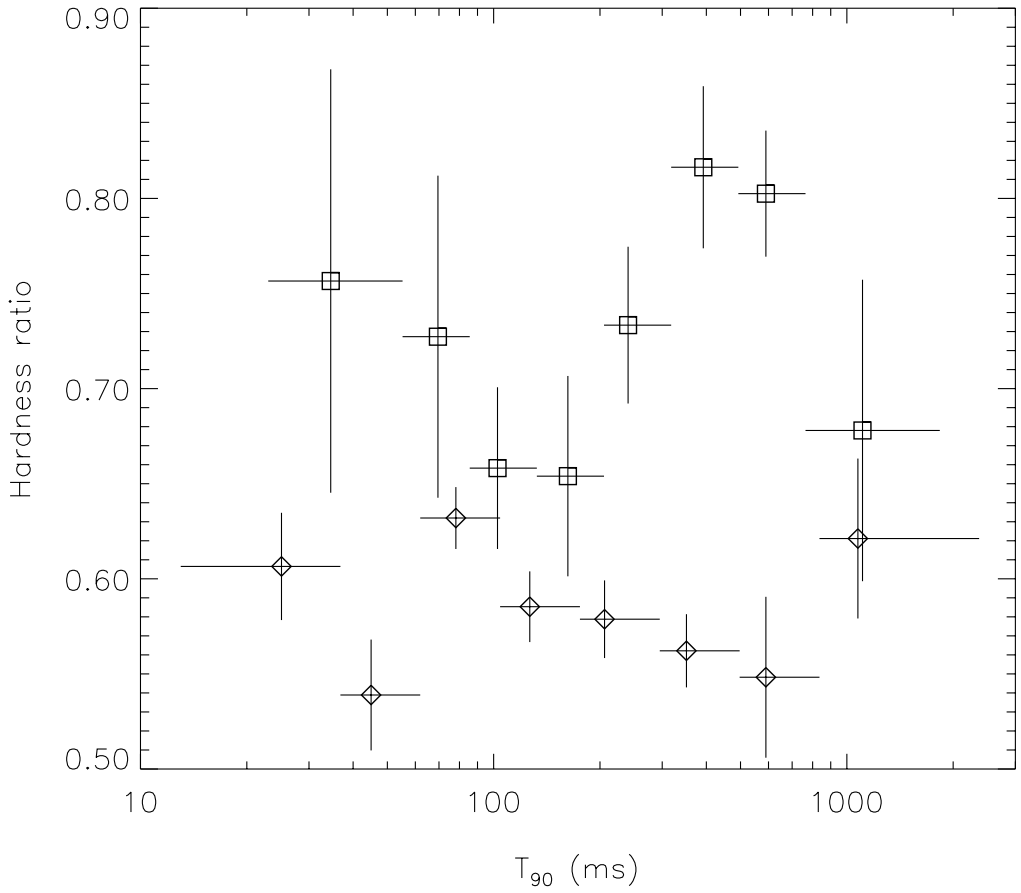

Fig. 11.— Plot of hardness ratios vs T_{90} durations for SGR 1806−20 bursts (squares) and for SGR 1900+14 (diamonds).